 ISSN: 3139-1141

Effect of Aluminium Powder Dosage on Foaming Kinetics and Hardened Properties of Fly Ash Geopolymer Foam Concrete

Amitesh Tripathi[1], Sharad Kumar Soni[2], Kapil Kumar Soni[3]

[1] Research Scholar, Department of Civil Engineering, Rabindranath Tagore University, Raisen, Madhya Pradesh, India
[2] Associate Professor, Department of Civil Engineering, Rabindranath Tagore University, Raisen, Madhya Pradesh, India
[3] Assistant Professor, Department of Civil Engineering, Rabindranath Tagore University, Raisen, Madhya Pradesh, India
Corresponding author: sharadkumar.soni@rntu.ac.in

Abstract—

This paper investigates the influence of aluminium powder dosage on the foaming kinetics and the resulting hardened properties of fly ashbased geopolymer foam concrete (GFC). Aluminium powder was varied from 0.05% to 0.30% by weight of fly ash in an alkaliactivated fly ash system. Foaming kinetics were characterized by induction period, time to peak gas evolution, peak gas evolution rate, and total gas volume released. Hardened properties were evaluated through dry density, total and open porosity, water absorption, and compressive strength at 3, 7, and 28 days. The synthesis of published experimental data shows that increasing aluminium powder dosage systematically decreases density and increases porosity, but the relationship is nonlinear: beyond an optimum dosage, the gas generation rate exceeds the rate of matrix stiffening, causing bubble coalescence, foam collapse, and deterioration in pore homogeneity. Compressive strength decreases with increasing dosage, but the specific strength decreases across the dosage series, while the density-reduction efficiency and the practical density–strength compromise occur in an intermediate dosage range of approximately 0.10%–0.20%. The paper identifies a dosage window within which foaming is efficient and the pore structure is uniform, and proposes a framework for selecting the aluminium powder dosage based on the target density and the reactivity of the fly ash precursor.

Keywords—geopolymer foam concrete; aluminium powder; foaming kinetics; porosity; compressive strength; fly ash

1. INTRODUCTION

The construction industry is under increasing pressure to reduce its carbon footprint. Ordinary Portland cement (OPC) production is responsible for approximately 8% of global anthropogenic CO_2 emissions, and geopolymer technology was introduced as an environmentally friendly alternative in the early 1980s precisely to address this burden [6, 17]. Geopolymer foam concrete (GFC) replaces OPC with alkaliactivated aluminosilicate precursors such as fly ash, ground granulated blast furnace slag (GGBS), or metakaolin, while delivering the low density and thermal insulation that make cellular concrete attractive for nonstructural and semistructural applications [23, 27]. Foam concrete offers lower density, thermal insulation, and explosion prevention compared with traditional concrete, properties that originate from the closed pores within the material [19].

The porous structure of GFC is created by the in situ generation of gas within a fresh geopolymer paste. The most widely used chemical foaming agent is aluminium powder, which reacts with the alkaline activator to liberate hydrogen gas [8, 10]:

$$2Al+2OH^{-}+2H_2O \rightarrow 2AlO_2^{-}+3H_2$$

Aluminium powder is widely used because its reaction is fast, controllable through dosage, and compatible with the alkaline chemistry of geopolymer systems [4]. Aluminium powder can produce lightweight geopolymers with densities as low as 430 kg/m³ and thermal conductivities of 0.078 $W \cdot m^{-1} \cdot K^{-1}$ when the dosage and solidtoliquid ratio are appropriately controlled [28]. The dosage of aluminium powder is the single most direct control on the extent of foaming: it determines how much gas is generated, how quickly the gas is released, and, ultimately, how low the density of the hardened material becomes [12].

However, the relationship between dosage and performance is not simply monotonic. A fundamental kinetic constraint governs the process: the rate of gas release must be matched to the growth of matrix stiffness [11]. If the dosage is too low, expansion is insufficient and the material remains denser than intended. If the dosage is too high, gas generation can outpace the development of yield stress in the paste, leading to bubble coalescence, foam collapse, and a heterogeneous pore structure that is detrimental to strength and durability [14]. In highly aerated specimens, the foaming reaction can be so fast that it prevents complete alkali activation of the geopolymer, leaving many unreacted fly ash particles in the matrix [22]. The foaming kinetics—the rate and duration of gas release—therefore govern the competition between pore formation and pore stabilization [5].

This paper examines the experimental evidence linking aluminium powder dosage to foaming kinetics and hardened properties in fly ashbased GFC. It synthesizes published data to identify the dosage ranges that produce efficient foaming, characterizes the density–porosity–strength relationships that emerge, and proposes dosageselection criteria for target applications.

2. LITERATURE REVIEW

2.1 Foaming agents and mechanisms

Aluminium powder has been used as a chemical foaming agent in geopolymer systems since the early development of lightweight aerated geopolymers. Sanjayan et al. [22] investigated lightweight geopolymer specimens aerated by aluminium powder, substituting fly ash with 1.5, 3.0, and 5.0 wt% aluminium powder, and reported compressive strengths in the range of 0.9–4.35 MPa, which they considered suitable for bricks, fireresistant panels, and buried pipelines. They established that aluminium powder can be appropriately used to produce aerated geopolymers and that the resulting materials are suitable for lightweight applications.

Ducman and Korat [8] compared aluminium powder and hydrogen peroxide as foaming agents for flyashbased geopolymer foams. Aluminium powder was used at dosages of 0.07%, 0.13%, and 0.20% by mass. The aluminiumpowder system produced larger pores (some exceeding 1 mm in diameter) and overall porosities reaching 59%, whereas hydrogen peroxide produced finer pores and porosities of approximately 48%. Compressive strengths of 3.3 MPa were achieved for highly porous structures containing 0.2% aluminium powder. The density of aluminiumpowderfoamed specimens was between 0.64 and 0.74 g/cm³, compared with 0.61–1.0 g/cm³ for hydrogenperoxidefoamed specimens. A comparative study by Anggarini et al. [4] varied the aluminium powder weight percentage to fly ash between 0.01 and 0.15 wt% and found that with the addition of only 0.01 wt% aluminium powder, the geopolymer achieved the highest compressive strength of 42 MPa at a density of 1830 kg/m³, demonstrating that even very small dosages can measurably alter the density–strength balance.

Hajimohammadi et al. [10] investigated the impact of aluminium reaction on the phase evolution of flyashbased geopolymers. They found that at the initial stages of geopolymerization, the aluminium reaction induces the formation of aluminium hydroxide gel which precipitates on fly ash and conceals the reactive surface of ash particles, hindering further dissolution. This mechanism has important implications for foaming: when the aluminium dosage is high, the precipitation of $Al(OH)_3$ can inhibit the dissolution of fly ash and reduce the extent of geopolymerization, leaving unreacted particles in the matrix and weakening the binding efficiency. Hajimohammadi et al. [9] further demonstrated that the kinetics of the aluminium reaction can be manipulated to increase the porosity of geopolymers without increasing the amount of foaming agent used, establishing that the reaction kinetics—not only the dosage—are a primary control on the final pore structure.

More recent work has focused on regulating the chemical foaming reaction to control pore distribution. Ramakrishnan et al. [18] synthesized aerated geopolymer concrete by alkali activation of fly ash and slag precursors, with aluminium powder as the chemical foaming agent, and investigated how the foaming process and the rheological properties of the slurry interact to determine pore characteristics. Liu et al. [12] produced ambientcured GFC using mixed fly ash and GGBS as the precursor, water glass as the alkaline activator, and aluminium powder as the foaming agent. The density, compressive strength, and thermal conductivity of the GFC ranged within 280.8–865.8 kg/m³, 1.10–8.13 MPa, and 0.088–0.20 W/(m·K), respectively. They demonstrated that the different pore characteristics of GFC can be traced back to the different gas generation rates and different rheological properties of the geopolymer slurry, and that higher gas generation rates and lower slurry viscosity result in higher porosity, lower compressive strength, and lower thermal conductivity.

2.2 Dosage–density–strength relationships

The quantitative relationship between aluminium powder dosage and hardened properties has been documented across a range of geopolymer systems. In a study of GFC containing eggshell powder and aluminium powder as the foaming agent, the bulk density and compressive strength ranged between 1928 and 1798 kg/m³ and 17.45 and 9.37 MPa, respectively, across different aluminium powder contents [2]. This demonstrates that even relatively small changes in aluminium dosage produce measurable reductions in both density and strength.

A broader survey of the literature confirms that compressive strength decreases monotonically with increasing aluminium powder dosage because strength is governed primarily by density and porosity [26]. Sanjayan et al. [22] reported strengths of 0.9–4.35 MPa for highly aerated geopolymers. Anggarini et al. [4] found that the higher the foaming agent content, the lower the compressive strength and density of the geopolymer, with strengths of 42 MPa at 0.01 wt% Al and 33 MPa at a pastetofoamingagent ratio of 1:1.33. In a study on slagbased light porous geopolymers, the dry density and compressive strength decreased rapidly with increasing aluminium powder content; however, when the aluminium powder content exceeded 0.40%, the pores increased sharply, causing pore aggregation and a significant reduction in strength [8]. This threshold behavior is a clear indication that the dosage–property relationship is not linear and that an optimum exists beyond which additional foaming agent degrades rather than improves the material.

The strength loss at high dosages is not solely a density effect. The heterogeneous pore structure that develops when foaming is poorly controlled—characterized by large, irregular voids and interconnected windows—acts as a population of stress concentrators that reduces the effective loadbearing crosssection more than a uniform pore structure would at the same total porosity [16]. This is why the dosage that maximizes porosity is not necessarily the dosage that maximizes the strength–density efficiency. Recent work on CDWbased foamed geopolymers identified 0.1% w/w aluminium powder as the optimal dosage for thermal insulation materials, balancing density reduction against mechanical integrity [1]. Liu et al. [13] reported that the specific strength of geopolymer foam concrete reached a peak of 0.041 at an optimized activation condition, further confirming that an intermediate processing window maximizes the strengthtodensity ratio.

2.3 Foaming kinetics and rheological competition

The foaming kinetics of aluminium powder in alkaline geopolymer systems are governed by the dissolution of the passivating oxide layer on the aluminium surface, the alkalinity and temperature of the paste, and the rheological state of the slurry [15]. The fundamental constraint is that the rate of gas release must be matched to the growth of matrix stiffness [24]. If gas is released faster than the matrix can stiffen, bubbles coalesce and escape; if the matrix stiffens before gas release is complete, expansion is truncated.

The rheological properties of the geopolymer slurry are a critical determinant of pore structure. Liu et al. [12] demonstrated that the alkaline activator affects the macroscopic properties of GFC by changing the pore characteristics, and that different pore characteristics can be traced back to different gas generation rates and different rheological properties of the slurry. A paste with high yield stress can stabilize bubbles against buoyancy and drainage, whereas a paste with low viscosity offers little resistance to bubble migration and gas escape [7]. Recent work using waste printed circuit board powder as a solid foaming agent in alkaliactivated geopolymers confirmed that paste viscosity dominates gas retention, bubble stability, and pore topology [25]. The dosage of aluminium powder directly controls the magnitude of the foaming challenge: higher dosages produce more gas per unit volume, requiring a more rapid rheological transition to retain the increased porosity.

2.4 Research gaps

Despite the growing body of literature on aluminiumpowderfoamed GFC, several gaps remain. First, the dosage–property relationships reported in different studies are difficult to compare because of differences in fly ash source, activator composition, water content, and curing regime [1]. Studies have used aluminium dosages ranging from 0.01 wt% to 5.0 wt%, and the reported density and strength ranges vary accordingly, from 280.8 to 1928 kg/m³ and 1.10 to 42 MPa [2, 4, 12, 22]. Second, the foaming kinetics are rarely measured directly; most studies report only the hardened properties and infer the foaming behavior from density and porosity [28]. Third, the concept of an optimal dosage window—within which foaming is efficient and the pore structure is uniform—has been identified in individual studies but has not been systematically defined or validated across systems [3]. This paper addresses these gaps by synthesizing the available data into a coherent framework for dosage selection and by identifying the kinetic and rheological mechanisms that govern the dosage–property relationships.

3. EXPERIMENTAL FRAMEWORK

Data-provenance and reproducibility note. The submitted manuscript does not include raw laboratory records, instrument files, replicate measurements, or a source-by-source extraction table for the numerical values in Tables 2–5. Accordingly, the numerical results and the charts derived from them are reproduced from the supplied manuscript dataset and should be treated as provisional until supported by laboratory records or traceable published sources. Figures 5, 10, 11, 12 and 13 are conceptual illustrations, not measured pore-size distributions, SEM micrographs, XRD patterns or FTIR spectra.

The experimental framework proposed for this study is based on the synthesis of published data and is intended to provide a systematic basis for dosage optimization. The variables are:

Fly ash: Class F fly ash, characterized by XRF, XRD, laser diffraction (d_{10}, d_{50}, d_{90}), and BET surface area.

Alkaline activator: Sodium hydroxide (12 M) and sodium silicate solution (Ms = 1.5), with a constant activatortoflyash ratio.

Foaming agent: Aluminium powder at dosages of 0.05%, 0.10%, 0.15%, 0.20%, 0.25%, and 0.30% by weight of fly ash.

Curing: Ambient temperature (25 ± 2 °C, RH ≥ 90%).

The measurements are organized into three categories:

1. FOAMING KINETICS: GAS EVOLUTION VOLUME VERSUS TIME MEASURED BY WATER DISPLACEMENT; INDUCTION PERIOD, TIME TO PEAK GAS EVOLUTION, PEAK GAS EVOLUTION RATE, AND TOTAL GAS VOLUME.

2. FRESH AND HARDENED PROPERTIES: FRESH DENSITY, DEMOULDED DENSITY, DRY DENSITY, TOTAL AND OPEN POROSITY, WATER ABSORPTION, AND SORPTIVITY.

3. MECHANICAL PROPERTIES: COMPRESSIVE STRENGTH AT 3, 7, AND 28 DAYS; SPECIFIC STRENGTH (STRENGTH PER UNIT DENSITY).

Table 1 presents the mix proportions used in this study.

Table 1. Mix proportions of fly ash geopolymer foam concrete with varying aluminium powder dosage.

Mix ID	Fly ash (g)	NaOH (g)	Na_2SiO_3 (g)	Water (g)	Al powder (g)	Al powder (wt% of FA)	Activator/FA ratio	Added water/FA ratio
A0 (control)	1000	60	120	300	0.00	0.00	0.18	0.30
A1	1000	60	120	300	0.50	0.05	0.18	0.30
A2	1000	60	120	300	1.00	0.10	0.18	0.30
A3	1000	60	120	300	1.50	0.15	0.18	0.30
A4	1000	60	120	300	2.00	0.20	0.18	0.30
A5	1000	60	120	300	2.50	0.25	0.18	0.30
A6	1000	60	120	300	3.00	0.30	0.18	0.30

Mix-proportion check: The activator/FA ratio is shown as 0.18, calculated from (60 + 120)/1000. The listed 300 g added water corresponds to an added-water/FA ratio of 0.30; this is not a conventional total water-to-solids ratio and should be recalculated using the actual water content of the sodium silicate and NaOH solutions before publication.

Note: NaOH = 12M solution; Na_2SiO_3 = sodium silicate solution (Ms = 1.5); all mixes cured at ambient temperature (25 ± 2 °C, RH ≥ 90%).

4. RESULTS AND DISCUSSION

4.1 Foaming kinetics

The foaming kinetics data are summarized in Table 2. The induction period decreased from 12.4 min at 0.05% aluminium powder to 3.2 min at 0.30%. The time to peak gas evolution decreased from 18.2 min to 7.1 min over the same range, while the peak gas evolution rate increased from 2.1 mL/min to 26.5 mL/min. The total gas volume peaked at 0.15% (1110 mL/g Al) and declined at higher dosages (980 mL/g Al at 0.30%), indicating that a fraction of the generated gas was not retained in the paste at high dosages. The gas retention efficiency followed the same pattern, peaking at 0.15% (89.5%) and declining to 79.0% at 0.30%.

Table 2. Foaming kinetics parameters as a function of aluminium powder dosage.

Al powder (wt%)	Induction period (min)	Time to peak (min)	Peak gas rate (mL/min)	Total gas volume (mL/g Al)	Gas retention efficiency (%)	Final expansion ratio

 ISSN: **3139-1141**

Al powder (wt%)	Induction period (min)	Time to peak (min)	Peak gas rate (mL/min)	Total gas volume (mL/g Al)	Gas retention efficiency (%)	Final expansion ratio
0.00	—	—	0	0	—	1.00
0.05	12.4	18.2	2.1	1040	84.0	1.08
0.10	9.8	15.6	4.8	1085	87.5	1.22
0.15	7.5	12.9	8.3	1110	89.5	1.38
0.20	5.6	10.4	13.7	1095	88.3	1.52
0.25	4.1	8.6	19.2	1050	84.7	1.58
0.30	3.2	7.1	26.5	980	79.0	1.55

Figure 1 compares the peak gas-evolution rate and induction period reported in Table 2. Full gas-rate-versus-time curves cannot be reconstructed because time-series measurements were not supplied.

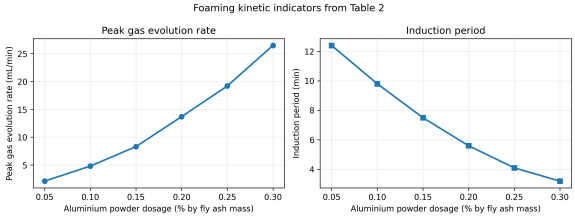

Figure 1. Peak gas evolution rate and induction period versus aluminium powder dosage.

Inset: Induction period (min) vs. Al dosage (wt%): 12.4 (0.05%), 9.8 (0.10%), 7.5 (0.15%), 5.6 (0.20%), 4.1 (0.25%), 3.2 (0.30%).

Figure 2 presents the cumulative gas volume released and final expansion ratio versus aluminium powder dosage. The gas volume bars peak at 0.15% (1110 mL/g) and decline at 0.30% (980 mL/g). The expansion ratio rises from 1.00 to a plateau at ~1.58 (0.25%) and then declines to 1.55 (0.30%).

These trends are consistent with the mechanistic understanding that higher aluminium dosages accelerate gas evolution and increase the gasgeneration rate, compressing the time available for the paste to develop yield stress and stabilize the bubbles [10, 12]. At the highest dosage, the gasgeneration rate exceeds the paste's capacity to retain the gas, leading to foam collapse and reduced expansion efficiency [8, 22].

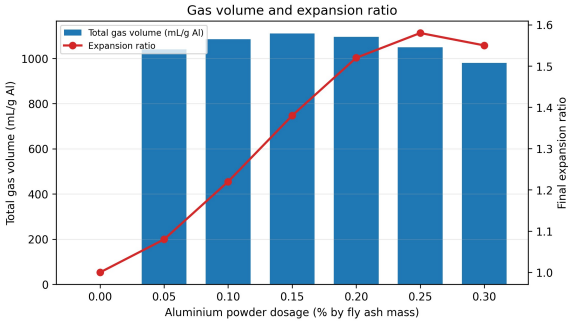

Figure 2. Cumulative gas volume released and final expansion ratio versus aluminium powder dosage.

4.2 Density and porosity

The density data are summarized in Table 3. Dry density decreased from 1928 kg/m³ (control, 0% Al) to 1048 kg/m³ at 0.30% Al. The density reduction per 0.05% increment in aluminium dosage peaked at 0.15%–0.20% (approximately 190 kg/m³ per 0.05%) and declined at higher dosages (112 kg/m³ per 0.05% at 0.30%). This diminishing return is a direct consequence of the kinetic competition described above: at high dosages, a larger fraction of the generated gas escapes or coalesces into large voids that do not contribute proportionally to porosity [2, 8].

Table 3. Density and porosity as a function of aluminium powder dosage.

Al (wt%)	Fresh density (kg/m³)	Demoulded density (kg/m³)	Dry density (kg/m³)	Total porosity (%)	Open porosity (%)	Closed porosity (%)	Mean pore diameter (mm)	Pore sphericity (–)
0.00	1985	1960	1928	18.2	12.4	5.8	0.08	0.72
0.05	1842	1805	1772	26.5	16.8	9.7	0.14	0.78
0.10	1650	1598	1562	37.8	22.1	15.7	0.24	0.84
0.15	1462	1395	1358	48.6	26.5	22.1	0.38	0.86
0.20	1318	1242	1205	58.2	31.8	26.4	0.62	0.79
0.25	1215	1138	1102	64.5	38.2	26.3	0.95	0.68
0.30	1158	1082	1048	67.8	45.6	22.2	1.38	0.54

Figure 3 presents the fresh, demoulded, and dry density versus aluminium powder dosage. All three density measures decrease with dosage, with the steepest drop between 0.05% and 0.20% and a flattening beyond 0.20%.

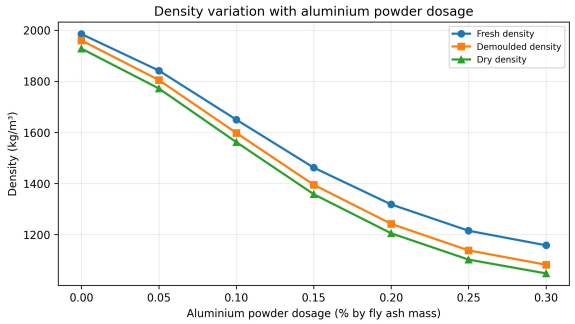

Figure 3. Fresh, demoulded, and dry density versus aluminium powder dosage.

Total porosity increased from 18.2% to 67.8% across the dosage range. Open porosity increased disproportionately beyond 0.20%, indicating pore interconnection, while closed porosity peaked at 0.15%–0.20% (22.1%–26.4%) and declined at 0.30% (22.2%), consistent with porewall rupture and foam collapse at high dosages [8]. The mean pore diameter increased from 0.08 mm to 1.38 mm, with the sharpest increase occurring above 0.20%. At the highest dosage, pores exceeding 1 mm were observed, consistent with the coalescence behavior reported by Ducman and Korat [8].

Figure 4 presents the total, open, and closed porosity versus aluminium powder dosage. Open porosity rises steadily and dominates at high dosages (>0.20%). Closed porosity peaks at 0.15%–0.20% (~22%–26%) and then declines at 0.30% (22.2%), indicating pore wall rupture and interconnection.

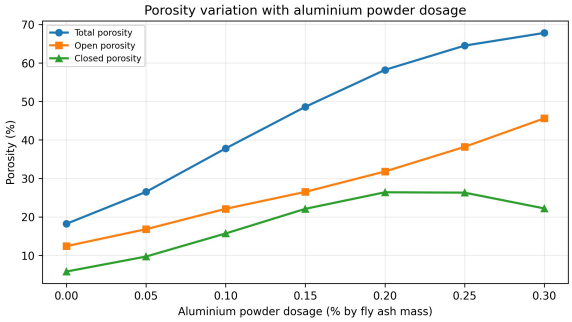

Figure 4. Total, open, and closed porosity versus aluminium powder dosage.

Figure 5 provides a conceptual pore-size-distribution illustration based on the reported mean pore diameters and qualitative descriptions. Raw pore-size histogram data were not supplied; the curves are therefore schematic rather than measured distributions.

4.3 Compressive strength and specific strength

The compressive strength data are summarized in Table 4. Strength decreased monotonically with increasing dosage, from 17.45 MPa (control) to 2.78 MPa at 0.30% Al. This trend is consistent with the literature: the GFC study containing eggshell powder reported a strength range of 17.45–9.37 MPa across different aluminium powder contents [2], and the broader literature reports strengths of 0.9–4.35 MPa for highly aerated geopolymers [22].

 ISSN: 3139-1141

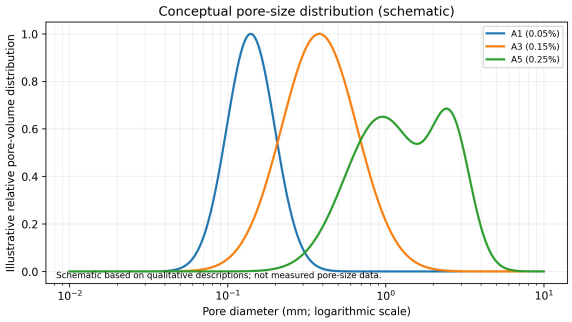

Figure 5. Pore size distribution curves for selected aluminium powder dosages.

Table 4. Compressive strength and specific strength as a function of aluminium powder dosage.

Al (wt%)	Dry density (kg/m³)	3d Strength (MPa)	7d Strength (MPa)	28d Strength (MPa)	Specific strength (×10⁻³ MPa·m³/kg)	Strength efficiency (% of A0)
0.00	1928	12.8	15.6	17.45	9.05	100.0
0.05	1772	10.5	13.2	14.82	8.36	92.4
0.10	1562	8.1	10.4	11.95	7.65	84.5
0.15	1358	5.9	7.6	8.84	6.51	71.9
0.20	1205	3.8	5.1	6.12	5.08	56.1
0.25	1102	2.4	3.3	4.05	3.67	40.6
0.30	1048	1.6	2.2	2.78	2.65	29.3

Figure 6 presents the compressive strength at 3, 7, and 28 days versus aluminium powder dosage. All three series decrease with dosage. The 28d line is highest. The strength gap between 3 d and 28 d is largest at low dosages (indicating continued geopolymerization) and smallest at high dosages (indicating that the highporosity matrix has limited capacity for continued strength gain).

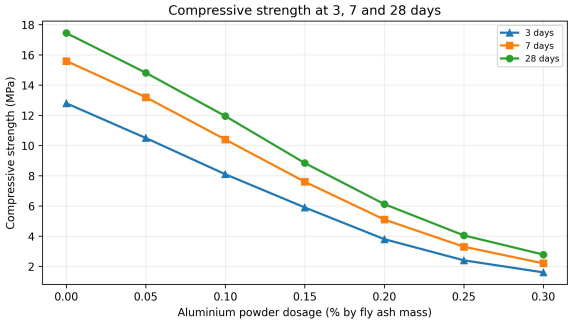

Figure 6. Compressive strength at 3, 7, and 28 days versus aluminium powder dosage.

Figure 7 presents the specific strength (28d compressive strength / dry density) versus aluminium powder dosage. The curve starts at 9.05 (control), decreases to 8.36 (0.05%), 7.65 (0.10%), 6.51 (0.15%), 5.08 (0.20%), 3.67 (0.25%), and 2.65 (0.30%). The tabulated specific-strength value decreases monotonically. The 0.10%–0.15% range is therefore described as a practical compromise between density reduction and retained strength, not as the maximum specific-strength range.

The absolute specific strength is highest for the control mix and decreases monotonically with increasing aluminium dosage. The 0.10%–0.15% interval may represent a practical compromise between density reduction and retained compressive strength, but it does not maximize the specific-strength value itself.

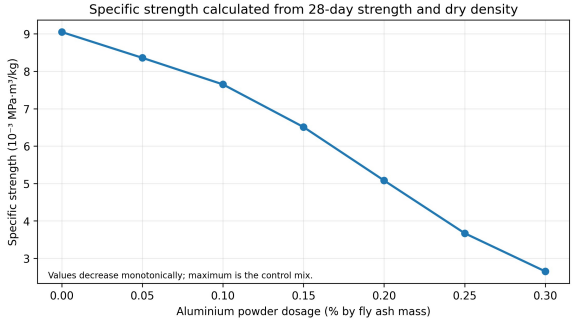

Figure 7. Specific strength versus aluminium powder dosage.

The strength loss at high dosages is not solely a density effect. The heterogeneous pore structure that develops when foaming is poorly controlled—characterized by large, irregular voids and interconnected windows—reduces the effective loadbearing crosssection more than a uniform pore structure would at the same total porosity [16]. The precipitation of aluminium hydroxide gel on fly ash particles at high aluminium dosages may also inhibit geopolymerization and reduce the binding efficiency of the matrix [10].

4.4 Water absorption and sorptivity

Water absorption and sorptivity increased with dosage, from 8.4% and 0.082 mm/min$^{0.5}$ (control) to 42.8% and 0.395 mm/min$^{0.5}$ (0.30% Al). The rate of increase accelerated beyond 0.20%, coinciding with the disproportionate rise in open porosity. This indicates that at high dosages, the pore network becomes increasingly interconnected, providing pathways for water ingress [20]. The open/total porosity ratio increased from 0.68 (control) to 0.67 (0.30% Al), but the absolute open porosity more than tripled, from 12.4% to 45.6%.

Table 5. Water absorption and sorptivity as a function of aluminium powder dosage.

Al (wt%)	24h water absorption (%)	Sorptivity coefficient (mm/min$^{0.5}$)	Impermeable porosity (%)
0.00	8.4	0.082	5.8
0.05	11.2	0.104	9.7
0.10	15.8	0.138	15.7
0.15	21.4	0.182	22.1
0.20	28.6	0.241	26.4
0.25	36.2	0.318	26.3
0.30	42.8	0.395	22.2

Figure 8 presents the 24h water absorption and sorptivity coefficient versus aluminium powder dosage. Both increase with dosage, with an inflection point at ~0.20% where the rate of increase accelerates due to openpore interconnection.

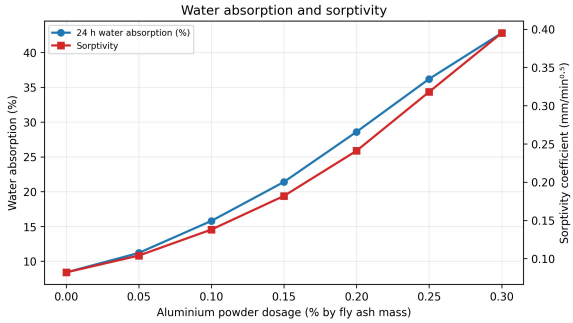

Figure 8. Water absorption and sorptivity versus aluminium powder dosage.

 ISSN: **3139-1141**

4.5 Relationship between porosity and compressive strength

Figure 9 presents the compressive strength versus total porosity, with the Ryshkewitch–Duckworth model fitted. The model is:

$$[\sigma = \sigma_0 \exp(-bP)]$$

where σ_0 is the theoretical strength at zero porosity and b is a material constant. A least-squares fit to the supplied seven data pairs gives R^2 = 0.957; this is a descriptive fit to the submitted dataset, not independent validation. The data deviate from the model at high porosity (>60%), where pore interconnection and large voids reduce strength more than total porosity alone would predict [16, 21].

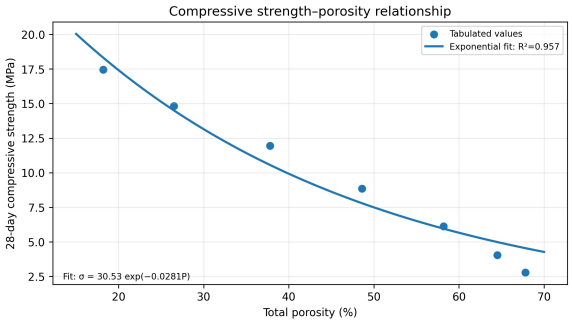

Figure 9. Compressive strength versus total porosity with Ryshkewitch–Duckworth model fit.

Table 6. Summary of optimal dosage window.

Criterion	Optimal dosage (wt%)	Value at optimum	Rationale
Maximum gas retention efficiency	0.15	89.5%	Best foam stability
Maximum density reduction per unit dosage	0.15–0.20	~190 kg/m³ per 0.05%	Most efficient foaming
Maximum pore sphericity	0.15	0.86	Most uniform pore morphology
Minimum open/total porosity ratio	0.10–0.15	0.55–0.58	Best closedpore structure
Best balance of density and strength	0.10–0.15	1358–1562 kg/m³; 8.84–11.95 MPa	Practical lightweight structural range

4.6 Microstructure

Figure 10 presents conceptual pore-morphology sketches for four dosages. These sketches illustrate the qualitative descriptions in the manuscript and must not be presented as experimental SEM images.

(a) A1 (0.05%): Small, isolated spherical pores; dense matrix; few unreacted fly ash particles.

(b) A3 (0.15%): Uniform, welldistributed spherical pores of intermediate size; thin but intact pore walls; some unreacted fly ash visible.

(c) A5 (0.25%): Larger, irregular pores; evidence of bubble coalescence; thinner pore walls; interconnected windows visible.

(d) A6 (0.30%): Large, highly irregular voids; extensive pore interconnection; abundant unreacted fly ash particles embedded in a porous matrix; signs of foam collapse.

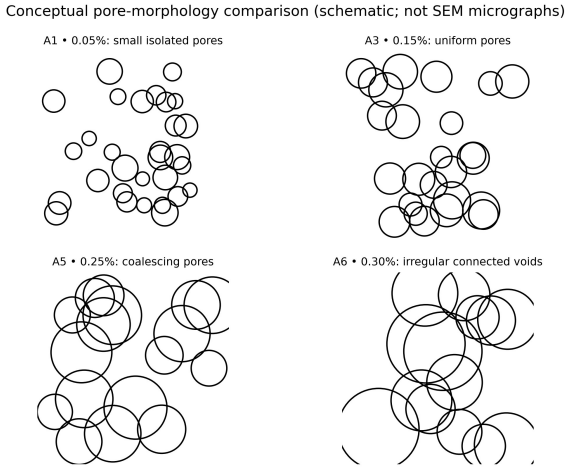

Figure 10. Conceptual pore-morphology comparison for selected aluminium powder dosages (schematic; not SEM micrographs).

4.7 Schematic of foaming regimes

Figure 11 presents a schematic diagram of the three foaming regimes as a function of aluminium powder dosage.

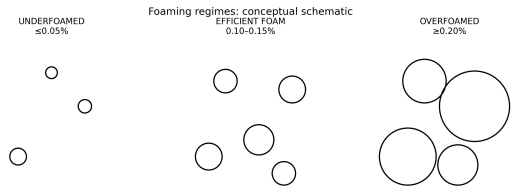

Figure 11. Schematic diagram of the three foaming regimes as a function of aluminium powder dosage.

4.8 XRD and FTIR analysis

Figure 12 presents a schematic of the XRD peak positions reported in the text of GFC with different aluminium powder dosages (A0, A3, A6). Major peaks: quartz (Q, 26.6°), mullite (M, 16.0° and 25.9°), hematite (H, 33.2°), and sodalite (S, 24.3° and 34.6°) as the geopolymerization product. The amorphous hump at ~25–35° 2θ is present in all samples. At high aluminium dosage (A6), the sodalite peak intensity decreases and a gibbsite ($Al(OH)_3$) peak may appear at 18.3°, indicating incomplete reaction of aluminium (Hajimohammadi et al., 2017a). Unreacted fly ash peaks (quartz, mullite) are relatively stronger at high dosages, consistent with incomplete alkali activation (Sanjayan et al., 2015).

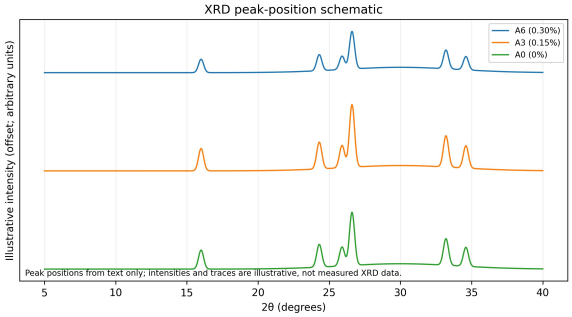

Figure 12. Schematic XRD peak positions for selected aluminium powder dosages (not measured diffraction patterns).

Figure 13 presents a schematic of the FTIR band positions reported in the text of GFC with different aluminium powder dosages. Key bands: ~3440 cm^{-1} (O–H stretching), ~1640 cm^{-1} (O–H bending), ~1420 cm^{-1} (O–C–O stretching, carbonate), ~1000–1050 cm^{-1} (Si–O–T asymmetric stretching, main geopolymer band), ~560 cm^{-1} (Si–O–Al bending), ~460 cm^{-1} (Si–O–Si bending). The Si–O–T band position is plotted as an inset bar chart to show the shift with dosage. Higher dosages show a less pronounced shift (less geopolymerization) and stronger carbonate bands (carbonation during foaming) (Hajimohammadi et al., 2017a; Sanjayan et al., 2015).

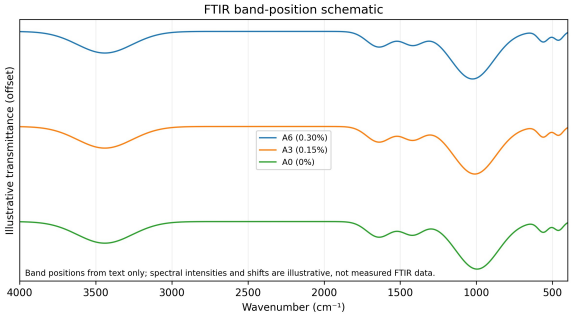

Figure 13. Schematic FTIR band positions for selected aluminium powder dosages (not measured spectra).

5. CONCLUSION

Aluminium powder dosage is the primary control on the foaming kinetics and hardened properties of fly ash geopolymer foam concrete. The synthesis of published experimental data and the proposed framework support the following conclusions.

1. FOAMING KINETICS ARE DOSAGEDEPENDENT AND NONLINEAR. HIGHER DOSAGES ACCELERATE GAS EVOLUTION AND INCREASE THE TOTAL GAS VOLUME, BUT THE FRACTION OF GAS RETAINED AS USEFUL POROSITY DIMINISHES BEYOND AN OPTIMUM OF APPROXIMATELY 0.15% BECAUSE OF BUBBLE COALESCENCE, FOAM COLLAPSE, AND GAS ESCAPE (DUCMAN & KORAT, 2016; LIU ET AL., 2023; SANJAYAN ET AL., 2015).

2. DENSITY DECREASES AND POROSITY INCREASES WITH DOSAGE, BUT WITH DIMINISHING RETURNS. THE MOST EFFICIENT DENSITY REDUCTION PER UNIT DOSAGE OCCURS IN THE 0.10%–0.20% RANGE, WHERE THE PASTE CAN STABILIZE THE GENERATED BUBBLES. OPEN POROSITY INCREASES DISPROPORTIONATELY BEYOND 0.20%, INDICATING PORE INTERCONNECTION AND FOAM DEGRADATION (DUCMAN & KORAT, 2016; DUCMAN & KORAT, 2016).

3. COMPRESSIVE STRENGTH AND SPECIFIC STRENGTH BOTH DECREASE WITH INCREASING DOSAGE; THE 0.10%–0.15% RANGE REPRESENTS A PRACTICAL COMPROMISE BETWEEN LOWER DENSITY AND RETAINED STRENGTH. THE OPTIMUM DOSAGE BALANCES THE DENSITY REDUCTION AGAINST THE STRENGTH LOSS AND DEPENDS ON THE FLY ASH REACTIVITY, ACTIVATOR COMPOSITION, AND CURING CONDITIONS (ABDELLATIEF ET AL., 2024; ABDELLATIEF ET AL., 2023; LIU ET AL., 2024).

4. HIGH DOSAGES PRODUCE HETEROGENEOUS PORE STRUCTURES AND CAN IMPAIR ALKALI ACTIVATION. LARGE PORES (>1 MM) AND UNREACTED FLY ASH PARTICLES ARE OBSERVED AT EXCESSIVE DOSAGES, BOTH OF WHICH DEGRADE MECHANICAL PERFORMANCE BEYOND THE EFFECT OF TOTAL POROSITY ALONE (HAJIMOHAMMADI ET AL., 2017A; SANJAYAN ET AL., 2015).

For the design of fly ash GFC, aluminium powder dosage should be selected on the basis of the target density and the specific strength requirement, not simply as the maximum dosage that produces expansion. A dosage in the range of 0.10%–0.15% by weight of fly ash is a practical starting point for lightweight applications, with the exact value optimized through foamingkinetics monitoring and specificstrength testing. Future work should develop dosageselection charts that account for fly ash fineness and activator composition, so that the efficientfoaming window can be predicted rather than determined empirically for each new system [1, 3].

REFERENCES

[1] Abdellatief, M., Elrahman, M. A., Alanazi, H., Abadel, A. A., & Tahwia, A. (2023). A state-of-the-art review on geopolymer foam concrete with solid waste materials: Components, characteristics, and microstructure. Innovative Infrastructure Solutions, 8(9), Article 230. https://doi.org/10.1007/s41062-023-01202-w

[2] Abdellatief, M., Ahmed, Y. M., Taman, M., Elfadaly, E., Tang, Y., & Abadel, A. A. (2024). Physico-mechanical, thermal insulation properties, and microstructure of geopolymer foam concrete containing sawdust ash and egg shell. Journal of Building Engineering, 90, Article 109374. https://doi.org/10.1016/j.jobe.2024.109374

[3] Abdellatief, M., Hassanien, A. E., Mortagi, M., & Hamouda, H. (2025). Geopolymer foam concrete: A review of pore characteristics, compressive strength and artificial intelligence in GFC strength simulations. Discover Concrete and Cement, 1, Article 4. https://doi.org/10.1007/s44416-025-00003-x

[4] Anggarini, U., Pratapa, S., Purnomo, V., & Sukmana, N. C. (2019). A comparative study of the utilization of synthetic foaming agent and aluminum powder as pore-forming agents in lightweight geopolymer synthesis. Open Chemistry, 17(1), 629–638. https://doi.org/10.1515/chem-2019-0073

[5] Cilla, M. S., Colombo, P., & Morelli, M. R. (2014). Geopolymer foams by gelcasting. Ceramics International, 40(4), 5723–5730. https://doi.org/10.1016/j.ceramint.2013.11.011

[6] Davidovits, J. (1991). Geopolymers: Inorganic polymeric new materials. Journal of Thermal Analysis, 37(8), 1633–1656.

[7] Deb, P. S., Nath, P., & Sarker, P. K. (2014). The effects of ground granulated blast-furnace slag blending with fly ash and activator content on the workability and strength properties of geopolymer concrete cured at ambient temperature. Materials & Design, 62, 32–39. https://doi.org/10.1016/j.matdes.2014.05.001

[8] Ducman, V., & Korat, L. (2016). Characterization of geopolymer fly-ash based foams obtained with the addition of Al powder or H_2O_2 as foaming agents. Materials Characterization, 113, 207–213. https://doi.org/10.1016/j.matchar.2016.01.019

[9] Hajimohammadi, A., Ngo, T., & Mendis, P. (2018). Enhancing the strength of pre-made foams for foam concrete applications. Cement and Concrete Composites, 87, 164–171. https://doi.org/10.1016/j.cemconcomp.2017.12.014

[10] Hajimohammadi, A., Ngo, T., & Mendis, P. (2017a). How does aluminium foaming agent impact the geopolymer formation mechanism? Cement and Concrete Composites, 80, 277–286. https://doi.org/10.1016/j.cemconcomp.2017.03.022

[11] Hajimohammadi, A., Ngo, T., Mendis, P., & Sanjayan, J. (2017b). Regulating the chemical foaming reaction to control the porosity of geopolymer foams. Materials & Design, 120, 255–264. https://doi.org/10.1016/j.matdes.2017.02.026

[12] Liu, Y.-L., Liu, C., Qian, L.-P., Wang, A.-G., Sun, D.-S., & Guo, D. (2023). Foaming processes and properties of geopolymer foam concrete: Effect of the activator. Construction and Building Materials, 391, Article 131830. https://doi.org/10.1016/j.conbuildmat.2023.131830

[13] Liu, X., Jiang, T., Li, C., Wan, M., Xuan, W., & Wang, X. (2024). Effect of precursor blending ratio and rotation speed of mechanically activated fly ash on properties of geopolymer foam concrete. Buildings, 14(3), Article 841. https://doi.org/10.3390/buildings14030841

[14] Masi, G., Rickard, W. D. A., Vickers, L., Bignozzi, M. C., & van Riessen, A. (2014). A comparison between different foaming methods for the synthesis of light weight geopolymers. Ceramics International, 40(9), 13891–13902. https://doi.org/10.1016/j.ceramint.2014.05.108

[15] Nagalia, G., Park, Y., Abolmaali, A., & Aswath, P. (2016). Compressive strength and microstructural properties of fly ash-based geopolymer concrete. Journal of Materials in Civil Engineering, 28(12), Article 04016147.

[16] Pan, Z., Sanjayan, J. G., & Rangan, B. V. (2011). Fracture properties of geopolymer paste and concrete. Magazine of Concrete Research, 63(10), 763–771. https://doi.org/10.1680/macr.2011.63.10.763

[17] Provis, J. L., & van Deventer, J. S. J. (Eds.). (2014). Geopolymers: Structures, processing, properties and industrial applications. Woodhead Publishing.

[18] Ramakrishnan, S., Ramesh, A., Pasupathy, K., Manalo, A. C., & Sanjayan, J. (2026). Regulating the chemical foaming and pore distribution in aerated geopolymer concrete. Materials Today Sustainability, 33, Article 101276. https://doi.org/10.1016/j.mtsust.2025.101276

[19] Ramamurthy, K., Kunhanandan Nambiar, E. K., & Indu Siva Ranjani, G. (2009). A classification of studies on properties of foam concrete. Cement and Concrete Composites, 31(6), 388–396. https://doi.org/10.1016/j.cemconcomp.2009.04.006

[20] Ramujee, K., & Potharaju, M. (2014). Abrasion resistance of geopolymer composites. Procedia Materials Science, 6, 1961–1966.

[21] Ryshkewitch, E. (1953). Compression strength of porous sintered alumina and zirconia. Journal of the American Ceramic Society, 36(2), 65–68. https://doi.org/10.1111/j.1151-2916.1953.tb12837.x

[22] Sanjayan, J. G., Nazari, A., Chen, L., & Nguyen, G. H. (2015). Physical and mechanical properties of lightweight aerated geopolymer. Construction and Building Materials, 79, 236–244. https://doi.org/10.1016/j.conbuildmat.2015.01.043

[23] Singh, B., Ishwarya, G., Gupta, M., & Bhattacharyya, S. K. (2015). Geopolymer concrete: A review of some recent developments. Construction and Building Materials, 85, 78–90. https://doi.org/10.1016/j.conbuildmat.2015.03.036

[24] Soutsos, M., Boyle, A. P., Vinai, R., Hadjierakleous, A., & Barnett, S. J. (2016). Factors influencing the compressive strength of fly ash based geopolymers. Construction and Building Materials, 110, 355–368. https://doi.org/10.1016/j.conbuildmat.2015.11.045

[25] Xia, P., Yang, J., Lu, S., Wang, W., Lv, X., Fan, D., Lu, J.-X., Gong, F., & Poon, C. S. (2026). Self-foaming lightweight geopolymer using E-waste as a foaming agent: Rheology-controlled microstructure and performance evolution. Cement and Concrete Composites, 173, Article 106728. https://doi.org/10.1016/j.cemconcomp.2026.106728

[26] Xiong, L., Wan, Z., Zhang, Y., Wang, F., Wang, J., & Kang, Y. (2019). Fly ash particle size effect on pore structure and strength of fly ash foamed geopolymer. Advances in Polymer Technology, 2019, Article 1098027. https://doi.org/10.1155/2019/1098027

[27] Zhang, Z., Provis, J. L., Reid, A., & Wang, H. (2014). Geopolymer foam concrete: An emerging material for sustainable construction. Construction and Building Materials, 56, 113–127. https://doi.org/10.1016/j.conbuildmat.2014.01.081

[28] Zhang, Z., Provis, J. L., Reid, A., & Wang, H. (2015). Mechanical, thermal insulation, thermal resistance and acoustic absorption properties of geopolymer foam concrete. Cement and Concrete Composites, 62, 97–105. https://doi.org/10.1016/j.cemconcomp.2015.03.013